PAPER

Halocuprate(I) zigzag chain structures with N-methylated DABCO cations – bright metal-centered luminescence and thermally activated color shifts†‡

Sebastian Maderlehner,§[a] Markus J. Leitl,§[b] Hartmut Yersin*[b] and Arno Pfitzner*[a]

Two compounds 1,4-dimethyl-1,4-diazoniabicyclo[2.2.2]octane *catena*-tetra-μ-halo-dicuprate(I) with DABCOMe$_2$ Cu$_2$X$_4$ (**1**: X = Br, **2**: X = I) were synthesized by hydrothermal reaction of copper(I) halides with the corresponding 1,4-diazoniabicyclo[2.2.2]octane (DABCO) dihydrohalides in an acetonitrile/methanol mixture. Both compounds crystallize monoclinically, **1** with a = 9.169(4) Å, b = 10.916(6) Å, c = 15.349(6) Å, β = 93.93(2)°, V = 1533(1) Å^3, Z = 4, space group $P2_1/n$ (no. 14) and **2** with a = 15.826(9) Å, b = 9.476(5) Å, c = 22.90(2) Å, β = 90.56(5)°, V = 3434(5) Å^3, Z = 8, space group $P2_1$ (no. 4), respectively (lattice constants refined from powder diffraction data measured at 293 K). The cations in both compounds are formed by *in situ* N-methylation of DABCOH$_2{}^{2+}$ cations by methanol in a S$_N$2 reaction. Both compounds contain an anionic copper(I) halide chain structure consisting of *trans* edge-sharing CuX$_4$ tetrahedra. The chains are strongly kinked at every 2nd junction thus forming a zigzag structure. The shortest halide–halide distances are observed between the halide ions of adjacent tetrahedra which are approaching each other due to the kinking. This structure type shows a specific luminescence behavior. Under optical excitation, the compounds exhibit yellow (**1**) and green (**2**) emission with photoluminescence quantum yields of Φ_{PL} = 52 and 4%, respectively, at ambient temperature. According to DFT and TDDFT calculations, the emission is assigned to be a phosphorescence essentially involving a metal centered transition between the HOMO consisting mainly of copper 3d and halide p orbitals and the LUMO consisting mainly of copper 4s and 4p orbitals. The temperature dependence of the emission spectra, decay times, and quantum yields has been investigated in detail, especially for **1**. From the resulting trends it can be concluded that the emission for $T \leq 100$ K stems from energetically lower lying copper halide segments. Such segments represent the structural motif of the halocuprate(I) chains. With increasing temperature energetically higher lying segments are populated which also emit, but open the pathway for thermally activated energy transfer to quenching defects.

Introduction

Halocuprates(I) are built from a very small number of building blocks which is in contrast to their structural diversity. One of these building blocks is the CuX$_4$-tetrahedron (X = Cl, Br, I). All types of linkage between tetrahedral units are observed including face-sharing with Cu–Cu distances shorter than in metallic copper.[1,2] This diversity is one reason for the rich structural chemistry of such materials. In the case of [P(C$_6$H$_5$)$_4$]$_2$[Cu$_2$I$_4$], four different polymorphs are known which contain two different conformers of the [Cu$_2$I$_4$]$^{2-}$ anion[3,4] and recently, a solvate of a tetraphenylphosphonium iodocuprate(I) containing acetone as solvent molecules was reported.[5] Furthermore, another tetraphenylphosphonium iodocuprate(I) containing a polyanion forming a helix built from CuI$_4$-tetrahedra has been reported.[6] A quite common structural motif in *catena*-cuprates(I) is a chain of *trans* edge-sharing tetrahedra. Several halocuprates(I) with this anionic structural feature are described in the literature.[7–15] Typical cations are alkali metals, ammonium, or even copper(II) which is coordinated by

[a]*Institute for Inorganic Chemistry, University of Regensburg, Universitätsstraße 31, 93053 Regensburg, Germany. E-mail: arno.pfitzner@ur.de; Fax: +49 941 943814551; Tel: +49 941 943 4551*

[b]*Institute for Physical Chemistry, University of Regensburg, Universitätsstraße 31, 93053 Regensburg, Germany. E-mail: hartmut.yersin@ur.de; Fax: +49 941 9434488; Tel: +49 941 943 4464*

four ammine[7] or two bidental ethylenediamine ligands.[8–10] The same complex anion containing *trans* edge-sharing tetrahedra was obtained with twofold protonated diamines such as ethylene diamine or piperazine as cations.[11] Bromocuprates(I) with similar structures were obtained with *N*-allylquinolinium,[12] *N*-allylmorpholinium,[13] 4-aminopyridinium,[14] and 2,6-diaminopyridinium[15] cations, respectively. All of these compounds can be classified into two groups depending on the arrangement of the tetrahedra within the halocuprate(I) complex anions, *i.e.* as stretched form, similar to the chains of tetrahedra in silicon disulfide,[16,17] and as a kinked chain at every 2nd junction causing a zigzag structure of the chain. An inverted chain structure with an N^{3-} anion in the center of the tetrahedra has been observed in lanthanide nitride halides,[18,19] lanthanide nitride tellurides[20] and alkali metal lanthanide halide tellurides.[21] Stretched anti-SiS$_2$ chains are observed within these compounds as well as kinked ones.

In situ N-alkylation of DABCO or other amines by methanol has been observed in high pressure experiments[22] and hydrothermal syntheses,[23–25] respectively. The use of DABCO and its protonated forms in halocuprate(I) syntheses has yielded a Cu$_4$I$_6$$^{2-}$ cluster with an *in situ* mono-methylated DABCO molecule,[25] and a 3D inorganic framework structure.[26] The crystal structure of **2** has recently been reported in a very brief form.[27] Structural data with higher quality are included in this paper.

The structural variability of halocuprate(I) and copper(I) halide clusters results in a rich diversity also in the luminescence properties, as many compounds emit visible light in different spectral regions upon optical excitation.[28–42,72,73] Although many studies have been performed during recent years on the emission behavior of Cu(I) complexes due to their potential for use as low-cost emitter materials for OLEDs,[36–45,68–72] only very limited investigations in this regard were carried out on copper-halide chains, such as the ones presented in this contribution.[46–48,73,75–77]

Herein, the syntheses, crystal structures, and photophysical properties of two new luminescent halocuprate(I) compounds containing chains of *trans* edge-sharing tetrahedra are presented and discussed. This structure type is connected with the occurrence of specific chain segments which largely determine the emission behavior as is elucidated, in particular, for compound **1**. Photophysical characterizations are carried out on the basis of detailed temperature-dependent studies of emission spectra, decay times, and quantum yields. DFT and TDDFT calculations were performed to complement the measurements. It was found that at low temperature the emission originates only from one type of chain segment. With increasing temperature, thermally activated energy transfer along the chain occurs to other chain segments and quenching states.

Experimental

[DABCOMe$_2$][Cu$_2$Br$_4$] (**1**) and [DABCOMe$_2$][Cu$_2$I$_4$] (**2**) were synthesized in a hydrothermal reaction. The freshly purified copper(I) halide[49] and DABCO dihydrobromide[50] or DABCO dihydroiodide monohydrate,[51] respectively, were weighed in a silica ampoule in a 1.8 : 1 ratio to achieve full conversion of the copper(I) halide. A typical reaction mixture contained 170 mg of the copper(I) halide and 180 mg (**1**) or 191 mg (**2**), respectively, of the corresponding DABCO dihydrohalide. Methanol (2.5 equivalents referring to DABCO·2HX (X = Br, I) and 1.5 mL acetonitrile were added as solvents. The ampoules were evacuated and sealed after freezing of the solvent with liquid nitrogen and were then transferred into a micro autoclave containing 5 mL of water to apply counter pressure. The reactions were performed at 150 °C for 5 days (**1**) or 130 °C for 14 days (**2**), respectively, yielding a pure product of colorless rod-like crystals in a 90% isolated yield referring to the amount of copper(I) halide. The rest of copper(I) halide remained in solution. Crystals suitable for single crystal X-ray structure determination were mounted on and glued to a glass fiber.

Diffraction data of **1** were collected on a STOE IPDS I (Mo-K$_\alpha$, λ = 0.71073 Å) at room temperature. Data were corrected for Lorentz and polarization effects and absorption was corrected numerically after a semi-empirical optimization of the crystal shape.[52] The structure was solved by direct methods using SIR92[53] followed by a full-matrix least-squares refinement with SHELXL97.[54] Hydrogen atom positions could be located from difference Fourier calculations and were refined without constraints but fixed U_{iso} = 0.035 Å^2 for methylene group hydrogen and 0.050 Å^2 for methyl group hydrogen, respectively.

Diffraction data of **2** were collected on an Xcalibur Ruby Gemini Ultra (Mo-K$_\alpha$, λ = 0.71073 Å) at 123 K. Data were corrected for Lorentz and polarization effects and a numerical absorption correction was performed after semi-empirical optimization of the crystal shape.[55] Solution and refinement of the structure were performed analogously to **1**. Hydrogen atoms were attached to the carbon atoms and refined with a riding model (HFIX 23 for methylene groups) and with circular Fourier (HFIX 137 for methyl groups), respectively. An isotropic displacement parameter U_{iso}(H) of 1.2 U_{eq}(C) (1.5 U_{eq}(C) for methyl group hydrogens) was constrained for the hydrogen atoms.[54] The single crystal used for data collection turned out to be twinned according to the matrix (-1 0 0, 0 -1 0, 0 0 1), *i.e.*, a twofold axis along *c*. Both domains showed racemic twinning due to the acentric space group. Proportions of the 4 domains refined to 45.6% for the main domain, 43.5% for the 2nd domain, 5.5% for the racemic twin of the main domain, and 5.4% for the racemic twin of the 2nd domain, respectively. Anisotropic refinement of carbon and nitrogen atoms did not provide any reasonable results. For this reason they were refined only with isotropic displacement parameters. Further crystallographic data and refinement details are displayed in Table 1.

Powder diffraction patterns of **1** and **2** were collected on a STOE STADI P (Cu-K$_{\alpha1}$, λ = 1.540598 Å) to confirm purity of the products, see ESI Fig. S1 and S2.‡ IR spectra of the products and the DABCO dihydrohalides were collected on a Varian Fourier transform Raman Module coupled to a Varian 670

Table 1 Crystal data and structure refinements for **1** and **2**

Compound	**1**	**2**
Empirical formula	$Br_4C_8Cu_2H_{18}N_2$	$C_8Cu_2H_{18}I_4N_2$
Formula weight	588.96	776.92
Crystal system	Monoclinic	Monoclinic
Space group	$P2_1/n$ (no. 14)	$P2_1$ (no. 4)
Unit cell dimensions[a]	$a = 9.169(4)$ Å	$a = 15.8121(2)$ Å
	$b = 10.916(6)$ Å; $\beta = 93.93(2)°$	$b = 9.4130(1)$ Å; $\beta = 90.011(1)°$
	$c = 15.349(6)$ Å	$c = 22.9117(3)$ Å
Volume, Z	1533(2) Å^3, 4	3410.16(7) Å^3, 8
Crystal size/mm^3	$0.2 \times 0.1 \times 0.07$	$0.25 \times 0.2 \times 0.15$
Density ρ_{calc}	2.552 g cm^{-3}	3.027 g cm^{-3}
Absorption coefficient $\mu(MoK_\alpha)$	13.179 mm^{-1}	9.717 mm^{-1}
Temperature	293 K	123 K
F_{000}	1112	2800
θ range for data collection	2.29 to 25.45°	3.08 to 28.70°
Limiting indices	$-11 \leq h \leq 11$, $-13 \leq k \leq 13$, $-18 \leq l \leq 18$	$-21 \leq h \leq 21$, $-12 \leq k \leq 11$, $-30 \leq l \leq 27$
Reflections collected	18 384	21 747
Independent reflections	2821 [$R_{int} = 0.0501$]	14 978 [$R_{int} = 0.0273$]
Data/restraints/parameters	2821/0/199	14 978/1/388
Goof S	1.040	1.038
Final R indices [$I > 2\sigma(I)$]	$R_1 = 0.0326$, w$R_2 = 0.0665$	$R_1 = 0.0337$, w$R_2 = 0.0756$
R indices (all data)	$R_1 = 0.0457$, w$R_2 = 0.0698$	$R_1 = 0.0340$, w$R_2 = 0.0759$
Weighting coefficients	$a = 0.0394$, $b = 0$	$a = 0.0302$, $b = 0$
$\Delta\rho_{min}$, $\Delta\rho_{max}$/e Å^{-3}	0.629, −0.482	1.078, −1.048

[a] Lattice constants of **1** were refined from powder diffraction data.

IR-FT-IR spectrometer using ATR technique to approve quantitative twofold N-methylation of the DABCO molecules within **1** and **2**, see ESI Fig. S3 and S4.‡ The IR-spectra were processed with the Varian Resolutions Pro software.[56]

NHC elemental analyses were performed on a Vario micro cube Elementar Analysensysteme GmbH and the calculated values match very well: **1** calculated: N 4.8%, H 3.1%, C 16.3%; found: N 4.8%, H 3.0%, C 16.5%; **2** calculated: N 3.6%, H 2.3%, C 12.4%; found: N 3.5%, H 2.3%, C 12.5%.

Emission and excitation spectra were recorded using a Fluorolog 3-22 (Horiba Jobin Yvon) spectrometer. Emission decay times were measured with a cooled photomultiplier (RCA C7164R) combined with a FAST ComTec multichannel scaler PCI card. For excitation, a pulsed Nd:YAG laser ($\lambda_{exc} = 355$ nm) was used and the signal was detected at the respective emission maximum. The temperature dependent measurements between 10 and 300 K (emission spectra and decay times) were recorded using a helium cryostat (Cryovac Konti Cryostat IT). For absolute measurements of the photoluminescence quantum yields, a Hamamatsu Photonics (C9920-02) system was used. For this, the excitation wavelength was set to $\lambda_{exc} = 350$ nm. DFT and TDDFT calculations were performed using the Gaussian09 software package. For all

calculations, the basis set LANL2DZ with an effective core potential was applied along with the B3LYP hybrid functional. The calculations were performed using the geometry obtained from X-ray diffraction measurements without further optimization.

Results and discussion

Crystal structures

Compounds **1** and **2** contain the tetra-μ-halo-dicuprate(I) polyanion consisting of exclusively edge-sharing CuX$_4$-tetrahedra (X = Br, I). These chains of tetrahedra are strongly kinked at every 2nd junction in **1** and **2** thus forming zigzag chains. The chains are arranged along [0 1 0] in **1** and along [0 0 1] in **2**, respectively, forming a hexagonal rod packing in both compounds. In **1**, all chains have the same alignment and are in an almost eclipsed conformation parallel to the chain direction. In contrast in **2**, the chains are arranged in an ABAB stacking along [1 0 0] and show a significant staggering parallel to the chain direction, see Fig. 1. The staggering causes a doubling of the translation period of the chains in **2**, see Table 1. The crystallographic data given in Table 1 show some clear differences between the compounds under discussion. This holds regardless of the fact that they contain the same cation and very similar polyanions. The lower symmetry of **2** is manifested by the staggering of the polyanions therein. This results in a symmetry reduction of the centrosymmetric space group $P2_1/n$ of **1** to the acentric space group $P2_1$ of **2** in combination with a doubling of the unit cell volume.

As mentioned above, a chain of tetrahedra kinked at every 2nd junction has already been reported in the literature.[7,12,20,27] This was observed in the N-allylquinolinium bromocuprate(I),[12] in the rubidium and ammonium iodocuprate(I) hydrates[7] and in the rare earth (RE) nitride tellurides RE$_4$N$_2$Te$_3$ (RE = La–Nd).[20] The diammonium and dirubidium bis(di-μ-iodo-cuprate(I)) hydrates[7] show a kinking comparable to that in **1** and **2**. Within the former, the distances d(I–I) between adjacent CuI$_4$-tetrahedra are shorter than some of the intra-tetrahedral distances d(I–I). The strong kinking results in short distances d(Cu–Cu) in the ammonium and rubidium iodocuprates(I)[7] as well as in the title compounds. The shortest distances of d(Cu–Cu) = 2.809(3) Å in $[(NH_4)_2(H_2O)][Cu_2I_4]$[7] and d(Cu–Cu) = 2.897(3) Å in $[Rb_2(H_2O)][Cu_2I_4]$[7] are slightly longer than the sum of the van der Waals radii[57] of 2.8 Å, whereas the shortest distances of d(Cu–Cu) = 2.740(2) Å in **1** and d(Cu–Cu) = 2.679(0) Å in **2** are significantly shorter. All these distances are longer than the distance d(Cu–Cu) of 2.556 Å in metallic copper.[58] This is not surprising since only those iodocuprates(I)[59–61] and bromocuprates(I)[62] containing face-sharing CuX$_4$-tetrahedra (X = Br, I) show distances d(Cu–Cu) in the range from 2.45 to 2.50 Å which are shorter than in metallic copper.[58] Structural details for the different halocuprates(I) and for La$_4$N$_2$Te$_3$ (as a representative for the RE-nitride tellurides) are given in Table 2.
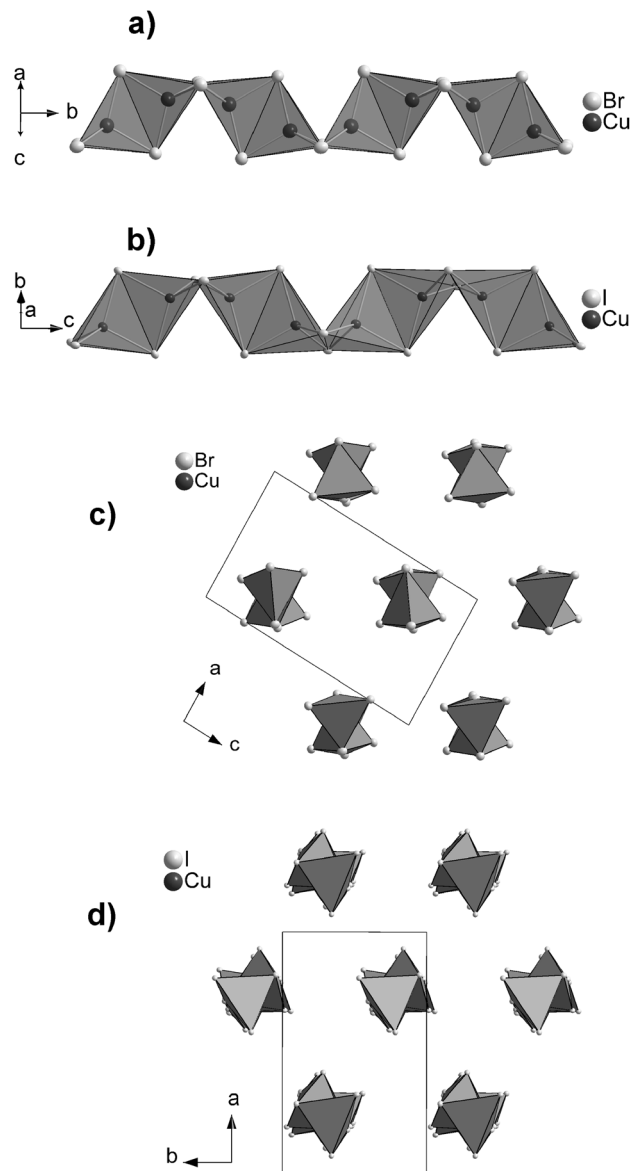
Fig. 1 Cu$_2$X$_4$ chains (X = Br, I) in **1** (a) and **2** (b) showing the strong kinking. Projections are displayed for **1** (c) and **2** (d) showing the hexagonal packing of the chains and the AB-stacking of two different orientations in **2**.

The chains in **1** and **2** show the strongest kinking in the series of compounds displayed in Table 2, since the shortest distances d(X–X) are observed between neighboring CuX$_4$-tetrahedra at the kinked junctions. A closer look at the angles ∠(X–Cu–X) and at the intra-tetrahedra distances d_{edge}(X–X) reveals significant distortions from an ideal tetrahedron within all compounds. The strongest distortion is found in the *N*-allylquinolinium compound due to a stretching of the bromocuprate(I) chain along the chain.[12] The dihedral angle between the faces of two undistorted edge-sharing tetrahedra should lie in the range from 66.0 to 70.5° to avoid distances d(X–X) at the kinking shorter than the intra-tetrahedron distances.[63] The dihedral angle between the faces is 62.0° in **1** and 62.1–63.3° in **2**.

The title compounds contain twofold *N*-methylated DABCO cations which take a staggered conformation with the dihedral angles ∠(N–C–C–N) of 14.8–16.5° in **1** and 0.8–16.4° in **2**, respectively. The cations are embedded between the anionic halocuprate(I) chains with each cation next to an almost planar face of a kinked junction, see Fig. 3. This figure shows that the space required by the cations matches the size of the plain face of the kinked tetrahedra junction quite well. In **1**, the cations have only one orientation with a small tilt of the N–N axis apart from the chain direction while in **2** the cations show two different orientations. One of them is similar to the orientation of the cations in **1** with a stronger tilt of the N–N axis. The second orientation is almost parallel to the chain direction, see Fig. 3. The tilted cations in **2** have a stronger staggered conformation with the dihedral angles ∠(N–C–C–N) of 10.0–16.4° than those oriented parallel to the chains with the dihedral angles ∠(N–C–C–N) of 0.8–4.5°.

The cations are formed by an *in situ* di-methylation of DABCO by methanol which is possible due to the enhanced pressure during the hydrothermal reaction, see Scheme 1.

It is well known that the size or volume per charge of the cation has a strong influence on the size and shape of the halocuprate(I) complex anion.[1,2,64] Sometimes choosing a particular cation allows for the prediction of the anionic structure.[65] The DABCOMe$_2^{2+}$ cations in **1** and **2** have a quite high charge density. The two positive charges of the molecular cation are located at the nitrogen atoms and are therefore very close to each other with distances d(N–N) of 2.56 Å in **1** and of 2.51 and 2.57 Å in **2**, respectively. Halocuprates(I) containing chains of edge-sharing CuX$_4$-tetrahedra have one negative

Table 2 Structural details of the tetrahedral chains $_\infty^1$[Cu$_2$X$_4^{2-}$] and $_\infty^1$[N$_2$RE$_4^{6+}$], respectively

Compound/cation	d(Cu–X)/Å	d(Cu–Cu)/Å	∠(X–Cu–X)/°	∠(Cu–X–X–Cu^a)/°	d(X–X^b)/Å	d(X–X^c)/Å
1	2.492–2.575	2.740–2.970	102–118	119	3.99–4.35	3.874
2	2.643–2.706	2.679–3.352	101–120	117–121	4.099–4.624	4.059–4.139
NH$_4^+$ (ref. 4)	2.631–2.697	2.809, 3.102	106–117	132–160	4.239–4.496	4.424–5.650
Rb$^+$ (ref. 4)	2.628–2.715	2.897, 3.098	107–118	133–157	4.281–4.518	4.511–5.730
N-Allyl-quinolinium[6]	2.50–2.623	3.305, 3.620	91–124	155	3.649–4.42	6.243
La$_4$N$_2$Te$_3$[11]	2.337–2.371	3.029, 3.106	96–118	146	3.525–4.070	4.718

^{a} Dihedral angle at the kinked junction. ^{b} Within the CuX$_4$ tetrahedra. ^{c} Between neighboring CuX$_4$ tetrahedra (X = Br, I), see Fig. 2.
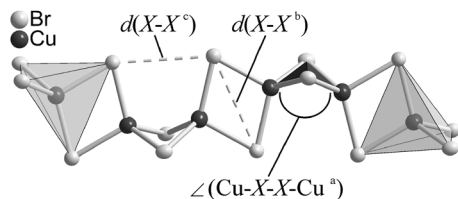
Fig. 2 Section of the chain structure in **1**. Distances and angles given in Table 2 are labeled.

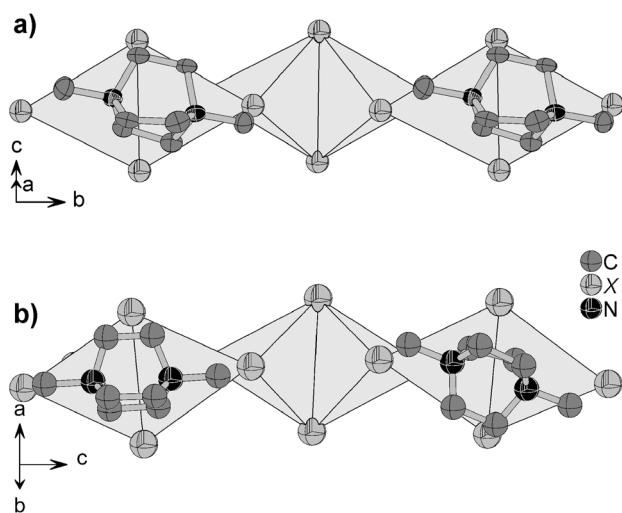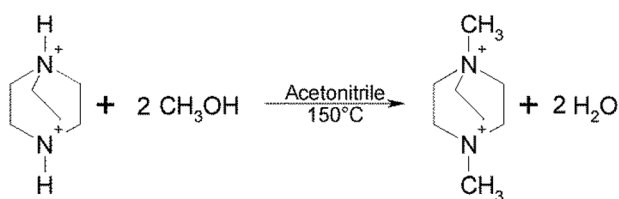**Fig. 3** Orientation of the cations in **1** (X = Br) (a) and **2** (X = I) (b) relative to the anionic chain structure, showing two alternating orientations in **2**. Hydrogen atoms are omitted for clarity.

Scheme 1 Twofold *N*-methylation of DABCO by methanol.

charge per tetrahedral unit. This means that each copper atom in **1** and **2** can be assigned to an adjacent nitrogen atom of the cation providing electroneutrality. The kinking of the junction might be a result of the short distances between the charges of the cations. A stretched Cu_2X_4-chain would lead to a reduced electrostatic interaction of the complex anion and the assigned cations.[66] Thus, the structure of the anion in **1** and **2** is mostly determined by the cations.

Photophysical properties

At ambient temperature, powders of the investigated compounds exhibit yellow (**1**) and green (**2**) luminescence, respectively, under optical excitation. The corresponding emission
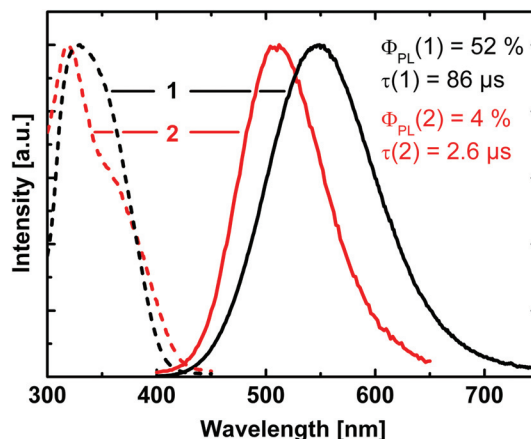

Fig. 4 Emission (solid lines) and excitation (dashed lines) spectra of **1** [DABCOMe₂][Cu₂Br₄] (black) and **2** [DABCOMe₂][Cu₂I₄] (red). The spectra were recorded from powders of the substances at ambient temperature (λ_{exc} = 350 nm). Φ_{PL} represents the emission quantum yield and τ the emission decay time.

spectra along with the excitation spectra are depicted in Fig. 4. The emission of compound **1** peaks at 550 nm, while it is significantly blue-shifted for compound **2** with a maximum at 510 nm. The emission decay times amount to τ = 86 μs (**1**) and τ = 2.6 μs (**2**), respectively. For the emission quantum yields Φ_{PL} values of 52% (**1**) and 4% (**2**) were found.

In the following discussion, we will focus on compound **1**. DFT and TDDFT calculations were performed to get an insight into the nature of the electronic transition(s) responsible for the luminescence. All calculations were restricted to segments of the copper halide chain which contain 2 copper and 4 bromide atoms. In this rather crude model, the periodicity of the system is neglected. From Fig. 2 (compare also Fig. 6), it can be seen that there are two types of such Cu_2Br_6 segments. In one type, the two central copper and the two central bromide atoms are arranged in a butterfly like shape (butterfly type, **A**) whereas in the other segment type these atoms are located in one plane (planar type, **B**). From the calculations it was found that the HOMOs for both types are located at the copper and bromide atoms, more specifically, the largest contributions to the HOMO stem from Cu 3d orbitals (≈60% (**A**), ≈70% (**B**)) and Br 4p orbitals (≈15% (**A**), ≈20% (**B**)). The LUMOs are mainly located on the copper atoms with the largest contributions stemming from 4s orbitals (≈55% (**A**), ≈60% (**B**)). TDDFT calculations reveal that mainly transitions between the frontier orbitals determine the first excited singlet (S_1) and triplet (T_1) states for both types of segments. Moreover, as the emission decay time at ambient temperature is of the order of almost 10^2 μs, the corresponding transition is assigned to be mainly metal-centered phosphorescence (^{3}(MC)) (with distinct halide contributions to the HOMO). The ground state is a singlet. This is in agreement with literature assignments of other, however molecular, halide copper systems.[28–35,46,67] Interestingly, the calculations give different transition energies for the T_1 states for the two seg-

ments differing by about 10^3 cm^{-1} (0.12 eV), with segment **A** being the energetically lower one.

The strong involvement of the Cu 3d orbitals in the HOMO might serve as an explanation for the observed blue shift of about 40 nm of the emission of compound **1** compared to that of **2**: the smaller ligand field strength of iodide compared to bromide results in a smaller splitting of the occupied Cu 3d orbitals. As a consequence, the HOMO of **1** is more destabilized than the HOMO of **2**. Thus, the emission of **1** appears at lower energy. Indeed, such a destabilization of the HOMO is also confirmed by the DFT calculations. Similar shifts of the emission energies have also been reported for other copper halide systems.[36,37,39]

For a more detailed understanding of the emission behavior, the samples were cooled to 10 K. With decreasing temperature, a significant unsymmetrical narrowing of the emission spectrum occurs for compound **1**. Formally, the emission spectrum is red-shifted from 545 to 575 nm (peak to peak) which is equivalent to about 960 cm^{-1} (0.12 eV), see Fig. 5. Interestingly, this energy difference is of about the same size as the one estimated from the TDDFT calculations for the transition energies of the two chain segments **A** and **B**. Therefore, it is indicated that at low temperature the emission originates from the chain segment which exhibits the lower transition energy. In the case of compound **1**, this is segment **A**. With increasing temperature, a thermal activation of segment **B** becomes possible, compare Fig. 6. Accordingly, a blue-shift and an unsymmetrical broadening of the emission spectrum are expected to occur upon heating. Indeed, this is observed experimentally. It is mentioned that in a recent report, a similar situation was described for a copper cyanide chain where the occurrence of different emission energies was also attributed to the existence of different chain segments.[48]

Moreover, the emission decay time of compound **1** was also investigated in dependence of the temperature, see Fig. 7.
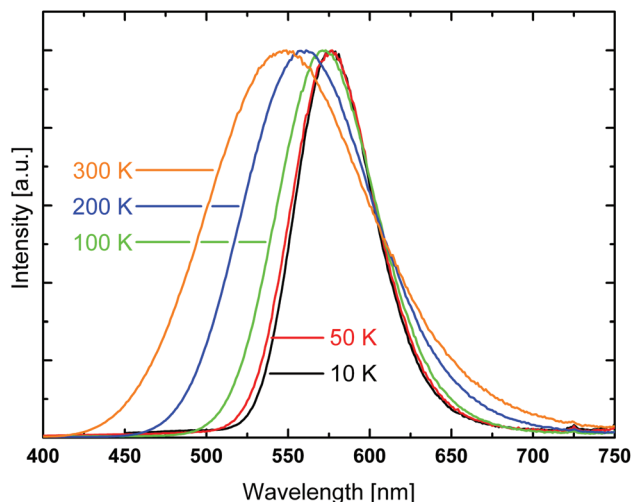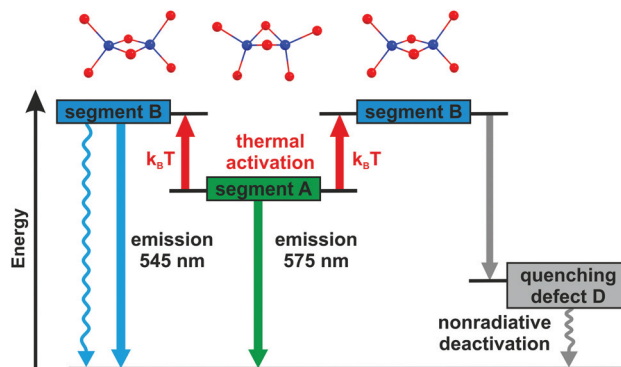

Fig. 6 Scheme of a proposed emission and quenching mechanism referring to compound **1**. At low temperatures (<50 K), only the energetically lower lying chain segments **A** emit. With increasing temperature, **B** segments can be thermally populated and emit at higher energy ($\approx 10^3$ cm^{-1}). However, according to the proposed mechanism, energy can also be transferred along chain segments and thus, reach unavoidable defect sites where the excitation can be deactivated nonradiatively. The structures of the respective chain segment types are displayed above the energy level diagram. Hereby, blue and red spheres represent copper and bromide atoms, respectively.
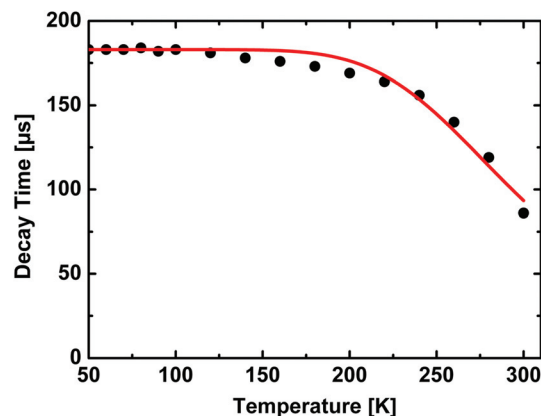

Fig. 7 Temperature dependent emission decay time of [DABCOMe$_2$]-[Cu$_2$Br$_4$] (**1**). As excitation light source a Nd:YAG laser with a wavelength of 355 nm was used. The red line represents a fit according to eqn (1).

Between 50 and about 100 K it amounts to about 180 μs. With further increase in temperature, the decay time decreases and reaches 86 μs at 300 K. Additionally, the quantum yields at 77 and 300 K were measured to be $\Phi_{PL}(77 K) = 85\%$ and $\Phi_{PL}(300 K) = 52\%$. This allows us to determine the radiative rates according to $k_r = \Phi_{PL}\tau^{-1}$. Within experimental error, the radiative rates k_r at 77 and 300 K ($k_r(77 K) = 5 \times 10^3$ s^{-1}, $k_r(300 K) = 6 \times 10^3$ s^{-1}) are equal. Therefore, the observed decrease of the emission decay time is a consequence of an increase of the nonradiative rate. This behavior can be rationalized by two different quenching mechanisms which are schematically displayed in Fig. 6. If the temperature is high enough, a thermally activated energy transfer between the chain segments can occur, presumably

Fig. 5 Emission spectra of [DABCOMe$_2$][Cu$_2$Br$_4$] (**1**) at different temperatures. Excitation wavelength λ_{exc} = 350 nm.

over a larger number of segments.¶ If so, the emission can be quenched by the defects in the chain structure (see Fig. 6, right-hand side).‖ Moreover, **B**-type chain segments themselves can exhibit an additional non-radiative decay channel to the ground state which becomes effective on thermal activation of these chain segments (see Fig. 6, left-hand side). Also, a combination of both effects can occur.

Thermally activated processes can (in the case of fast thermal equilibrium) be described by modified Boltzmann functions which are often found in the literature.[36,43–45] Eqn (1) represents an adaption of such a function to the system investigated in this contribution. Fitting this equation to the experimental data of decay time *versus* temperature, as shown in Fig. 7, allows us to estimate the activation energy for the quenching processes.

$$\tau(T) = \frac{1 + \exp\left[-\dfrac{\Delta E(A-B)}{k_B T}\right]}{\dfrac{1}{\tau(A)} + \left(\dfrac{1}{\tau(B)} + \dfrac{1}{\tau(D)}\right)\exp\left[-\dfrac{\Delta E(A-B)}{k_B T}\right]} \quad (1)$$

Herein, $\Delta E(A - B)$ represents the energy difference between segments **A** and **B** and therefore, the activation energy for the energy transfer, $\tau(A)$ and $\tau(B)$ are the emission decay times of segment **A** and segment **B**, respectively, $\tau(D)$ is the quenching constant for the non-radiative deactivation (*via* energy transfer to defect sites and quenching at segment **B**), and k_B is the Boltzmann constant. For this rough approach we assume that the population of segment **B** and the quenching process exhibit the same activation energy, as a determination of the rate constants of the individual processes of segment **B** and of the defect site D is not possible in the scope of our experiments.**

From fitting the data displayed in Fig. 7 with eqn (1) it is found that the activation energy amounts to about 1300 cm^{-1} (0.16 eV). This value is in reasonable agreement with the

values determined for the energy difference between the two segments by the TDDFT calculations ($\approx 10^3$ cm^{-1}) and the shift of the emission energy with temperature (≈ 960 cm^{-1}, Fig. 5). Further support for this model is given by the fact that the decrease of the emission decay time is paralleled by the broadening of the emission spectra above $T \approx 100$ K. Therefore, it is not unreasonable to assume that both effects are caused by the same activation mechanism.

For completeness, it is mentioned that the observed decrease of the emission decay time with increasing temperature is not in agreement with a thermally activated delayed fluorescence (TADF) which is often found for molecular copper compounds, as the decrease found here is a result of a thermally activated quenching mechanism in contrast to the population of a highly emissive singlet state in the TADF case.[36,37,39,43–45,69–71]

Conclusions

Two halocuprates(I) 1,4-dimethyl-1,4-diazoniabicyclo[2.2.2]-octane *catena*-tetra-µ-halo-dicuprate(I) with DABCOMe₂ Cu₂X₄ (**1**: X = Br, **2**: X = I) have been synthesized and characterized by single crystal X-ray diffraction and luminescence spectroscopy. The use of methanol as a high pressure methylation agent yields twofold *N*-methylated DABCO cations formed in an *in situ* S$_N$2-reaction similar to reactions under extreme conditions reported in the literature.[22–25] The influence of the cation size on the structure of the halocuprate(I) anion becomes obvious from their crystal structures: a polyanion built of edge-sharing CuX₄-tetrahedra (X = Br, I) is formed due to the high charge density of the DABCOMe₂$^{2+}$ cation. This is in perfect agreement with the tendency that highly charged cations yield polymeric halocuprate(I) anions with tetrahedrally coordinated copper atoms.[1,2]

The luminescence properties of both compounds were examined in detail. It was found that the emission results largely from a metal centered phosphorescence with distinct contributions of the halides to the HOMO. An analysis of the temperature dependence of the emission spectra, quantum yields, and of the decay times suggests for compound **1** that at low temperature, the emission originates only from an energetically lower lying segment of the [DABCOMe₂][Cu₂Br₄] chain, while with temperature increase, energy states of an energetically higher lying segment are populated. This opens the pathway for an energy transfer along the chain but also for non-radiative deactivation channels either at the higher energy segments themselves or by energy transfer to defect sites. The activation energy for this process was determined to be in the range of 1000–1300 cm^{-1} (0.12–0.16 eV).

Acknowledgements

¶ Cu(I) complexes often undergo distortions on excitation which leads to a trapping of the excitation energy on one specific emitter molecule and therefore, prohibits an efficient energy transfer to adjacent molecules.[36,37,43–45] In the case of the compounds presented in this contribution, it seems that this self-trapping mechanism and therefore the localization of the excitation energy at one chain segment is not effective (at ambient temperature) for two reasons. (i) Distortions in molecular Cu(I) complexes on excitation are related to a pronounced charge-transfer from the copper center to the ligand. This leads to a formal oxidation of the copper center and therefore to a geometry change from a pseudo-tetrahedral towards a more planar geometry. For the copper halide chains presented in this study the transitions are mainly metal-centered and therefore, charge-transfer and geometry distortions do not seem to be significant. (ii) Possible geometry distortions are further reduced as the emitting individual chain segments are embedded into the rigid framework of the entire chain.

‖ Defects might be represented by defects in the chain structure itself, boundary effects, or unavoidable impurities in real systems. Energy transfer along the chain is presumably occurring by a Dexter energy transfer process. A corresponding quenching mechanism was already suggested by Dexter and Schulman.[74]

** The degeneracy of the deactivating state(s) is not known and therefore, it is set to 1 in this rough estimate. Such a degeneracy factor has significant influence on the emission decay time but only minor influence on the activation energy. Therefore, only the activation energy is estimated.

References

1 C. Hasselgren Arnby, S. Jagner and I. Dance, *CrystEngComm*, 2006, **46**, 257.

2 S. Jagner and G. Helgesson, *Adv. Inorg. Chem.*, 1991, **37**, 1.

3 H. Hartl, I. Brüdgam and F. Mahdjour-Hassan-Abadi, *Z. Naturforsch., B: Anorg. Chem. Org. Chem.*, 1985, **40**, 1032.

4 A. Pfitzner and D. Schmitz, *Z. Anorg. Allg. Chem.*, 1997, **623**, 1555.

5 E. Jalilian, R.-Z. Liao, F. Himo, H. Brismar, F. Laurell and S. Lidin, *CrystEngComm*, 2011, **13**, 4729.

6 H. Hartl and F. Mahdjour-Hassan-Abadi, *Angew. Chem.*, 1994, **106**, 1929; H. Hartl and F. Mahdjour-Hassan-Abadi, *Angew. Chem., Int. Ed. Engl.*, 1994, **33**, 1841.

7 M. Hoyer and H. Hartl, *Z. Anorg. Allg. Chem.*, 1991, **598/599**, 151.

8 R. P. Hammond, D. J. Chesnut and J. A. Zubieta, *J. Solid State Chem.*, 2001, **158**, 55.

9 B. Freckmann and K. F. Tebbe, *Z. Naturforsch., B: Anorg. Chem. Org. Chem.*, 1980, **35**, 1319.

10 O. Simonsen and H. Toftlund, *Acta Crystallogr., Sect. C: Cryst. Struct. Commun.*, 1987, **43**, 831.

11 E. Redel, M. Fiederle and C. Janiak, *Z. Anorg. Allg. Chem.*, 2009, **635**, 1139.

12 A. V. Pavlyuk, V. N. Davydov and M. G. Mys'kiv, *Koord. Khim.*, 2003, **29**, 199.

13 E. A. Goreshnik and M. G. Mys'kiv, *Koord. Khim.*, 2003, **29**, 541.

14 J. Sertucha, A. Luque, F. Lloret and P. Román, *Polyhedron*, 1998, **17**, 3875.

15 S.-H. Liu, J.-D. Chen, L.-S. Liou and J.-C. Wang, *Inorg. Chem.*, 2001, **40**, 6499.

16 E. Zintl and K. Loosen, *Z. Phys. Chem.*, 1935, **174**, 301.

17 W. Büssem, H. Fischer and E. Gruner, *Naturwissenschaften*, 1935, **23**, 740.

18 S. Uhlandt and G. Meyer, *J. Alloys Compd.*, 1995, **225**, 171.

19 C. M. Schurz and Th. Schleid, *J. Alloys Compd.*, 2009, **485**, 110.

20 F. Lissner and Th. Schleid, *Z. Anorg. Allg. Chem.*, 2005, **631**, 1119.

21 C. M. Schurz and Th. Schleid, *J. Solid State Chem.*, 2010, **183**, 2253.

22 A. Olejniczak and A. Katrusiak, *CrystEngComm*, 2010, **12**, 2528.

23 Q. Hou, J.-J. Zhao, T.-Q. Zhao, J. Jin, J.-H. Yu and J.-Q. Xu, *J. Solid State Chem.*, 2011, **184**, 1756.

24 H. Chan, Y. Chen, M. Dai, C.-N. Lü, H.-F. Wang, Z.-G. Ren, Z.-J. Huang, C.-Y. Ni and J.-P. Lang, *CrystEngComm*, 2012, **14**, 466.

25 Q. Hou, X.-J. Qu, J. Jin, J.-J. Zhao, J.-H. Yu and J.-Q. Xu, *J. Cluster Sci.*, 2011, **22**, 715.

26 J. Song, Y. Hou, L. Zhang and Y. Fu, *CrystEngComm*, 2011, **13**, 3750.

27 J.-J. Hou, S.-L. Li, C.-R. Li and X.-M. Zhang, *Dalton Trans.*, 2010, **39**, 2701–2707.

28 N. P. Rath and E. M. Holt, *Inorg. Chem.*, 1985, **24**, 3934.

29 M. Vitale, W. E. Palke and P. C. Ford, *J. Phys. Chem.*, 1992, **96**, 8329.

30 P. C. Ford and A. Vogler, *Acc. Chem. Res.*, 1993, **26**, 220.

31 P. C. Ford, E. Cariati and J. Bourassa, *Chem. Rev.*, 1999, **99**, 3625.

32 M. Vitale and P. C. Ford, *Coord. Chem. Rev.*, 2001, **219–221**, 3–16.

33 C. K. Ryu, M. Vitale and P. C. Ford, *Inorg. Chem.*, 1993, **32**, 869.

34 E. Cariati and J. Bourassa, *Chem. Commun.*, 1998, 1623.

35 E. Cariati, X. Bu and P. C. Ford, *Chem. Mater.*, 2000, **12**, 3385.

36 M. J. Leitl, F.-R. Küchle, H. A. Mayer, L. Wesemann and H. Yersin, *J. Phys. Chem. A*, 2013, **117**, 11823–11836.

37 D. M. Zink, M. Bächle, T. Baumann, M. Nieger, M. Kühn, C. Wang, W. Klopper, U. Monkowius, T. Hofbeck, H. Yersin and S. Bräse, *Inorg. Chem.*, 2013, **52**, 2292–2305.

38 Z. Liu, P. I. Djurovich, M. T. Whited and M. E. Thompson, *Inorg. Chem.*, 2012, **51**, 230–236.

39 M. Wallesch, D. Volz, D. M. Zink, U. Schepers, M. Nieger, T. Baumann and S. Bräse, *Chem. – Eur. J.*, 2014, **20**, 6578.

40 Z. Liu, J. Qiu, F. Wei, J. Wang, X. Liu, M. G. Helander, S. Rodney, Z. Wang, Z. Bian, Z. Lu, M. E. Thompson and C. Huang, *Chem. Mater.*, 2014, **26**, 2368.

41 K. Tsuge, *Chem. Lett.*, 2013, **42**, 204–208.

42 P. C. Ford, *Coord. Chem. Rev.*, 2011, **132**, 129–140.

43 R. Czerwieniec, J. Yu and H. Yersin, *Inorg. Chem.*, 2011, **50**, 8293–8301.

44 H. Yersin, A. F. Rauch, R. Czerwieniec, T. Hofbeck and T. Fischer, *Coord. Chem. Rev.*, 2011, **255**, 2622–2652.

45 R. Czerwieniec, K. Kowalski and H. Yersin, *Dalton Trans.*, 2013, **42**, 9826–9830.

46 X. Liu, G.-C. Guo, A.-Q. Wu, L.-Z. Cai and J.-S. Huang, *Inorg. Chem.*, 2005, **44**, 4282–4286.

47 J.-K. Cheng, Y.-G. Yao, J. Zhang, Z.-J. Li, Z.-W. Cai, X.-Y. Zhang, Z.-N. Chen, Y.-B. Chen, Y. Kang, Y.-Y. Qin and Y.-H. Wen, *J. Am. Chem. Soc.*, 2004, **126**, 7796–7797.

48 C. Bayse, L. K. Harper, J. L. Ming and R. D. Pike, *Dalton Trans.*, 2014, **43**, 11243–11251.

49 A. Pfitzner, *Chem. – Eur. J.*, 2000, **6**, 1891.

50 M. Andrzejewski, A. Olejniczak and A. Katrusiak, *Cryst. Growth Des.*, 2011, **11**, 4892.

51 S. Maderlehner and A. Pfitzner, *Z. Kristallogr.*, 2012, **227**, 569.

52 *X-RED32*, STOE & Cie GmbH, Darmstadt, 2004; *X-SHAPE*, STOE & Cie GmbH, Darmstadt, 1999.

53 A. Altomare, G. Cascarano, C. Giacovazzo and A. Gualardi, *J. Appl. Crystallogr.*, 1993, **26**, 343.

54 G. M. Sheldrick, *Acta Crystallogr., Sect. A: Fundam. Crystallogr.*, 2008, **64**, 112.

55 *CrysalisPro software*, Version 1.171.35.11, Agilent Technologies, 2011.

56 *Resolutions Pro software*, Version 4.1.0.101, Molecular Spectroscopy Solutions, Varian Inc., 2006.

57 J. K. Nagle, *J. Am. Chem. Soc.*, 1990, **112**, 4741; A. Bondi, *J. Phys. Chem.*, 1964, **68**, 441–451.

58 W. L. Bragg, *Philos. Mag.*, 1914, **28**, 255.

59 A. K. Nurtaeva and E. M. Holt, *Acta Crystallogr., Sect. C: Cryst. Struct. Commun.*, 1998, **54**, 594.

60 H. Hartl and F. Mahdjour-Hassan-Abadi, *Angew. Chem.*, 1981, **93**, 804, (*Angew. Chem., Int. Ed.*, 1981, **20**, 772).

61 S. Andersson and S. Jagner, *Acta Chem. Scand., Ser. A*, 1985, **39**, 181.

62 W. Wang, L. Zhang, X.-B. Xu and Q. Ye, *Inorg. Chem. Commun.*, 2011, **14**, 626–631.

63 U. Müller, *Inorganic Structural Chemistry*, John Wiley & Sons Ltd, The Atrium, Southern Gate, Chichester, West Sussex PO19 85Q, England, 2nd edn, 2007.

64 E. Jalilian and S. Lidin, *CrystEngComm*, 2011, **13**, 5730.

65 S. Andersson, M. Håkansson and S. Jagner, *Inorg. Chim. Acta*, 1993, **209**, 195.

66 S. Lorenzo, C. Horn, D. Craig, M. Scudder and I. Dance, *Inorg. Chem.*, 2000, **39**, 401.

67 A. Vogler and H. Kunkely, *J. Am. Chem. Soc.*, 1986, **108**, 7211–7212.

68 M. J. Leitl, V. A. Krylova, P. I. Djurovich, M. E. Thompson and H. Yersin, *J. Am. Chem. Soc.*, 2014, **136**, 16032–16038.

69 R. Czerwieniec and H. Yersin, *Inorg. Chem.*, 2015, **54**, 4322–4327.

70 C. Linfoot, M. J. Leitl, P. Richardson, A. F. Rausch, O. Chepelin, F. J. White, H. Yersin and N. Robertson, *Inorg. Chem.*, 2014, **53**, 10854–10861.

71 T. Hofbeck, U. Monkowius and H. Yersin, *J. Am. Chem. Soc.*, 2015, **137**, 399.

72 F. Wu, J. Li, H. Tong, Z. Li, C. Adachi, A. Langlois, P. D. Harvey, L. Liu, W.-Y. Wong, W.-K. Wong and X. Zhu, *J. Mater. Chem. C*, 2015, **3**, 138–146.

73 F. Wu, H. Tong, Z. Li, W. Lei, L. Liu, W.-Y. Wong, W.-K. Wong and X. Zhu, *Dalton Trans.*, 2014, **43**, 12463–12466.

74 D. L. Dexter and J. H. Schulman, *J. Chem. Phys.*, 1954, **22**, 1063–1070.

75 G. Zeng, S. Xing, X. Han, B. Xin, Y. Yang, X. Wang, G. Li, Z. Shi and S. Feng, *R. Soc. Chem. Adv.*, 2015, **5**, 40792–40797.

76 Y. Song, R. Fan, P. Wang, X. Wang, S. Gao, X. Du, Y. Yang and T. Luan, *J. Mater. Chem. C*, 2015, **3**, 6249–6259.

77 M. Knorr, A. Bonnot, A. Lapprand, A. Khatyr, C. Strohmann, M. M. Kubicki, Y. Rousselin and P. D. Harvey, *Inorg. Chem.*, 2015, **54**(8), 4076–4093.